



Global Brain Involvement in Posterior Cortical Atrophy: Multimodal MR Imaging Investigation

Haya Glick-Shames¹ · Tarek Keadan¹ · Yael Backner¹ · Atira Bick¹ · Netta Levin¹

Received: 11 January 2020 / Accepted: 23 July 2020 / Published online: 6 August 2020
© Springer Science+Business Media, LLC, part of Springer Nature 2020

Abstract

Posterior cortical atrophy (PCA), considered a visual variant of Alzheimer's disease, has similar pathological characteristics yet shows a selective visual manifestation with relative preservation of other cortical areas, at least at early stages of disease. Using a gamut of imaging methods, we aim to evaluate the global aspect of this relatively local disease and describe the interplay of the involvement of the different brain components. Ten PCA patients and 14 age-matched controls underwent MRI scans. Cortical thickness was examined to identify areas of cortical thinning. Hippocampal volume was assessed using voxel-based morphometry. The integrity of 20 fiber tracts was assessed by Diffusion Tensor Imaging. Regions of difference in global functional connectivity were identified by resting-state fMRI, using multi-variant pattern analysis. Correlations were examined to evaluate the connection between grey matter atrophy, the network changes and the disease load. The patients presented bilateral cortical thinning, primarily in their brains' posterior segments. Impaired segments of white matter integrity were evident only within three fiber tracts in the left hemisphere. Four areas were identified as different in their global connectivity pattern. The visual network-related areas showed reduced connectivity and was correlated to atrophy. Right Broadman area 39 showed in addition increased connectivity to the frontal areas. Global structural and functional imaging pointed to the highly localized nature of PCA. Functional connectivity followed grey matter atrophy in visual regions. White matter involvement seemed less prominent, however damage is directly related to presence of disease and not mediated only by grey matter damage.

Keywords Posterior cortical atrophy (PCA) · Connectivity · Diffusion tensor imaging (DTI) · Cortical thickness · And functional MRI

Introduction

Posterior Cortical Atrophy (PCA) was first described by Benson as a disorder with decline in visual function and atrophy of posterior cortical areas (Benson et al. 1988). PCA is considered a visual variant of Alzheimer's disease (AD) (Beh et al. 2015; Alladi et al. 2007). The primary clinical manifestations

at onset mostly involve visual disorders. However, with the progression of disease, full dementia usually emerges. Pervious research suggested that some memory deficits are even evident in the initial stages of the disease (Ahmed et al. 2016, 2018). In 2017 a consensus classification for the syndrome extended its definition to include, in addition to the classic definition (PCA-core), features of other neuro-degenerative syndromes (PCA-Plus) and underlying pathologies other than Alzheimer's (Crutch et al. 2017). However, the classic PCA-pure attributable to AD, at least at presentation, is considered a localized disease affecting high-order visual areas, both in the dorsal (Shames et al. 2015) and ventral (Migliaccio et al. 2016) visual streams. The local aspects of the disease have been studied extensively in both grey and white matter. Voxel-based morphometry (VBM) research has pointed to atrophy of the parieto-occipital regions (Peng et al. 2016; Montembeault et al. 2018). Similarly, single-photon emission computed tomography (SPECT) showed that gradual decrease

Handling Editor: Christoph M. Michel.

Electronic supplementary material The online version of this article (<https://doi.org/10.1007/s10548-020-00788-z>) contains supplementary material, which is available to authorized users.

✉ Netta Levin
netta@hadassah.org.il

¹ fMRI Lab, Neurology Department, Hadassah-Hebrew University Medical Center, POB 12000, Jerusalem 91120, Israel

in metabolism begins posteriorly in the parietal lobes and then spreads to include the occipital lobes (Kas et al. 2011). The impact on neighboring white matter was also assessed using diffusion tensor imaging (DTI) methods pointing to reduced fiber integrity of both high and low visual pathways (Migliaccio et al. 2012; Cerami et al. 2015; Glick-Shames et al. 2018), as well as in the posterior cingulate and in the splenium and body of the corpus callosum (Caso et al. 2015; Madhavan et al. 2016; Agosta et al. 2018). In addition, functional connectivity within the visual networks was shown to be reduced (Lehmann et al. 2015; Migliaccio et al. 2016; Glick-Shames et al. 2018).

Memory-related structures have also been shown to be affected. Hippocampal atrophy was described in later stages of the disease (Manning et al. 2015) and others have pointed to the involvement of the precuneus volume as well (Ahmed et al. 2018). Functional connectivity outside the visual network was studied mostly in context of the default mode network (DMN) (Lehmann et al. 2015; Migliaccio et al. 2016), known to be involved in AD (Son et al. 2017). A recent paper examining the functional connectome using graph theory found that PCA patients had alterations of both intra- and inter-hemispheric connections, exceeding the structural damage. These alterations also included frontal connections (Migliaccio et al. 2020).

Clinicians treating this population are frequently puzzled by the discrepancy between the relatively preserved memory, language and inter-personal functions in the face of reduced visual abilities. The selective nature of the disease supplies an ideal opportunity for investigating neuro-degenerative diseases, particularly those sharing Alzheimer's pathology. In the past, imaging studies in PCA primarily focused on grey matter effects in early-affected networks and regions, while the global aspects of the disease were studied to a lesser extent. Lately, research has turned to review global aspects of the disease as well. Herein, we too, attempted to examine the brain with a whole brain approach. We used a gamut of imaging measures in the entire brain to evaluate grey matter (using cortical thickness and voxel-based morphometry [VBM]), white matter (using whole brain tractography) and global functional connectivity (using RS-fMRI). Furthermore, we examined the relationships between these different imaging modalities, in order to evaluate the possible interplay between the involvement of different brain components. These results will allow to better describe the dynamics of damage and possible compensational mechanisms in this unique disease.

Methods (for Further Details, See Supplementary Methods)

Subjects

Ten PCA patients (four females), aged 63.3 ± 8.15 years (mean \pm SD) were assessed by a Neurologist (NL), based on the criteria described in the meta-analysis of Alves et al. (insidious onset of progressive decline in visual and spatial dysfunction in the absence of ophthalmological impairment or neuroimaging lesions. Cognitive ability and language should be mostly preserved (Alves et al. 2013)). These criteria also match the first two classification levels described by Crutch et al. (Crutch et al. 2017). Average time from initial symptoms was 2.88 ± 0.64 years. All patients were referred by neurologists.

Cognitive, language and visual test results, as well as PET and CSF tau assays, are described in Tables 1 and 2. Fourteen age-matched healthy volunteers (six females, aged 60.86 ± 7.17 years) were enrolled as a control group. *T*-tests showed no significant differences between groups in age, gender or education.

The Hadassah-Hebrew University Medical Center Ethics Committee approved the experimental procedure. Written informed consent was obtained for all subjects.

Structural MRI Data

MRI data were acquired on a 3-T scanner (four patients and six controls on Siemens Trio; six patients and five controls on Siemens Skyra) using a 32-channel standard head-coil. MRI sequences included high-resolution T1-weighted images (minimum echo time [TE], flip angle 9° , repetition time [TR] = 2300 ms, voxel size of $1 \times 1 \times 1$ mm).

For Cortical thickness we used the surface based analysis (SBM) in Computational Analysis Toolbox (CAT 12, Jena University hospital), an extension of SPM12 (Wellcome Department of cognitive Neurology).

Data were segmented into grey matter (GM), white matter (WM) and cerebral spinal fluid (CSF), and normalized to Montreal Neurological Institute (MNI) space. Data quality was checked for homogeneity (all scans were within one standard deviation of homogeneity). Then data was smoothed by a 15 mm kernel (using standard procedure and parameters for surface-based analysis). The cortical thickness of each hemisphere was compared between groups using *t*-test to identify significant areas of cortical thinning with a threshold of $p < 0.05$ (FWE). Scanner, age, total intracranial volume (TIV) and gender were added as covariates. Regions showing significant reduction in the patient group were defined as atrophied foci. The areas

Table 1 Patients information

#	Patient	Age (years)	Gender	Education (years)	Years from first symptom	FDG-PET	Tau pg/ml	Neuro-psychological evaluation	Visual tests					
									Lobes affected	MMSE	Language	Boston naming test (% recognized)	HRR color (% recognized)	Faces recognition (% recognized)
1	71	M	19	2.00	Occipital Parietal	–	28	100	100	100	100	90	12	100
2	81	F	19	3.17	–	–	29	92	100	100	100	83	9	100
3	55	M	12	2.92	–	–	25	83	100	100	100	50	12	100
4	61	F	16	3.17	–	–	19	81	100	100	100	50	12	40
5	66	M	16	2.83	Temporal	204	100	100	100	100	100	46	8	400
6	65	F	18	3.17	Parietal	–	25*	100	100	100	100	5	12	400
7	53	F	16	2.17	Occipital Parietal	–	23	100	100	100	100	30	8	200
8	61	M	16	2.33	Occipital Temporal Parietal	–	18	90	100	100	100	40	6	40
9	58	M	17	4.25	Occipital Parietal	835	29	88	100	100	100	100	7	70
10	62	M	22	2.83	–	–	29	88	100	100	100	100	7	70

PET positron emission tomography

*Cognitive test was done using montreal cognitive assessment (MOCA) score and was converted to MMSE according to conversion table based on (Bergeron et al. 2017)

Behavioral testing are described in detail in (Shames et al. 2015): cognitive testing was done using the mini-mental state examination (MMSE) (Folstein et al. 1975) scores range 0–30, a score less than 24 is considered impaired). Language was tested using the 60 item Boston naming test BNT (LaBarge et al. 1986). A score less than 85% is considered impaired

Vision tests: Color was tested using the Hardy-Rand-Rittler (HRR) pseudo isochromatic screening Plates 5–10 (Cole et al. 2006). A score less than 85% is considered impaired. Face recognition was tested using the 20 famous pictures test developed in lab 20 famous Israeli and international faces (Shames et al. 2015). A score less than 80% is considered impaired. Spatial recognition of direction was tested using gradually reduced percentage of coherent movement in a random dot array developed in our lab a score greater than 15% is considered impaired (Shames et al. 2015). Complex scene perception was tested using the cookie Theft (LaBarge et al. 2002) a score of less than 13 is considered impaired (Shames et al. 2015). Stereopsis perception was tested using the Randot Stereo-test, a score greater than 40" is considered impaired (Birch and Salomão, 1998)

Table 2 Control information

Control	Age	Gender	Educa- tion (years)
1	51	F	17
2	68	M	17
3	62	M	15
4	57	M	15
5	64	M	18
6	54	M	15
7	57	F	17
8	66	M	21
9	78	M	21
10	64	F	18
11	60	F	18
12	63	F	19
13	53	F	16
14	55	M	16

were identified using the Yale Atlas of Brodmann Areas (Lacadie et al. 2008).

ROIs for correlation analysis were defined using the LONI Probabilistic Brain Atlas (<https://www.loni.usc.edu/research/atlas>). The average cortical thickness of each subject was calculated in regions showing a significant between group difference ($p < 0.02$, Bonferroni corrected) including the bilateral Lateral Occipital regions (LO), the bilateral Inferior Parietal (IP) region, right Supramarginal gyrus (rSMG), right Lingual gyrus (rLG) and right Cuneus.

The Hippocampus volume was calculated for each individual with the predefined ROI of the hippocampus using the voxel-based morphometry tool in Computational Analysis Toolbox (CAT 12) and compared between groups using standard t -test. All volumetric statistical analyses were done using the statistical tools implemented in CAT 12.

DTI

DTI data were acquired using a diffusion-weighted imaging sequence, (single-shot, spin-echo, TE = 94 ms, TR = 7127–8224 ms, FOV = 260 × 260 mm, matrix = 128 × 128, 52–60 axial slices, 2-mm-thick slices, $b = 0$ and $b = 1000$ s/mm²). The high b -value was obtained by applying gradients along 64 different diffusion directions. DTI image processing and analysis was performed using the mrVista package (<https://vistalab.stanford.edu/software>). Preprocessing included removing eddy current distortions and subject motion. Data was registered and aligned to the T1 image using mutual information algorithm.

The preprocessed data were analyzed using *Automated Fiber Quantification* (AFQ) (Yeatman et al. 2012). The

DTI data of each scan underwent whole-brain tractography using deterministic algorithm. Then the data were segmented into 20 tracts: (Nine fibers were delineated in each hemisphere separately: Thalamic Radiations, Corticospinal, Cingulum-Cingulate, Cingulum-Hippocampus, Inferior Frontal Occipital Fasciculus, Inferior Longitudinal Fasciculus, Superior Longitudinal Fasciculus, Uncinate Fasciculus, and Arcuate Fasciculus; and two commissural fibers were analyzed bilaterally: Forceps Major and Minor. All were selected based on the previously defined Mori WM atlas (Wakana et al. 2007; Hua et al. 2008)). Each fiber was resampled 100 equidistant nodes and the fiber tract core was calculated as the mean of all fibers x , y , z coordinates at each node. Following, fibers were cleaned and stray fibers were removed using an iterative algorithm that removes fibers whose length is different in more than four standard deviations from the mean fiber length or five standard deviations distant from the core of the fiber tract, as detailed in Yeatman et al (Yeatman et al. 2012).

In order to avoid partial voluming with non-white matter, diffusion measurements were taken near the dense core of the fibers. Diffusion at the core was estimated by combining data in a weighted fashion, assigning greater weight to voxels that are close to the core of the estimated tract. Diffusion measures along the tract were re-sampled at 100 positions, calculating fractional anisotropy (FA), radial diffusivity and axial diffusivity, at each of these nodes. In this way, measures throughout the length of the fiber could be combined across different subjects. (Yeatman et al. 2012). To evaluate the hypothesis of microstructure changes in fiber integrity in the patient group, one directional t -tests were conducted point-wise along each fiber tract for 100 points for each parameter. Specifically, we hypothesized a decrease in FA and axial diffusivity and an increase in radial diffusivity. Familywise error (FWE) corrected alpha for pointwise comparisons and FWE corrected cluster size were calculated for each fiber at $p < 0.05$ to correct for multiple comparisons (Nichols and Holmes 2002). A between-group effect along the fiber was considered significant if it passed one of the two criteria for $p < 0.05$. The effect of MRI scanner type was directly tested in fibers that showed a significant group difference using standard t -test.

The average FA along the significant tracks (points 6–95, and 6-41/60-95 for bi-hemispheric fibers) were calculated for further between measure analysis.

It should be noted that the tracts chosen were those included in the AFQ package. As we aimed to evaluate global aspects of PCA, we chose to use this automatic tracking package that enables us to reconstruct many major tracts in the brain without prior assumptions.

Resting State fMRI

Resting state fMRI measurements were obtained with an echo-planar imaging sequence, (8 min, TR/TE = 2250/30 ms, FOV = 218 × 218 mm², matrix 64 × 64, 37 slices, slice thickness 3.4 mm). Functional images were co-registered to the anatomical images through trilinear interpolation and were transformed into MNI space (Evans et al. 1993). Functional preprocessing was conducted in two stages. The first part of the analysis was done using Conn toolbox (Whitfield-Gabrieli and Nieto-Castanon 2012) including: realignment and unwarp, functional outlier detection (ART-based detection of outlier scans for scrubbing), functional direct segmentation and normalization, structural segmentation and normalization, and functional smoothing. Then, the preprocessed functional images underwent de-noising steps, including de-noising for CSF and WM BOLD signal (five dimensions each), six realignment parameters and their 1st order temporal derivatives, scrubbing confounds and effect of rest.

A multivariate pattern analysis (MVPA) was conducted in order to locate clusters of voxels that showed greater between-group variability, height threshold $p < 0.001$ uncorrected and cluster threshold $p < 0.05$ FDR-corrected. Significant clusters from the MVPA were used in a post-hoc seed-based functional connectivity analysis using the BrainVoyager QX software package (Brain Innovation, Maastricht, The Netherlands). Each seed was demarcated as a 10 mm sphere (similar to the size of the clusters identified in the MVPA analysis) around the peak of the cluster. A standardized size for all seeds was chosen to allow comparison between connectivity maps. Individual connectivity maps from these seed regions were generated using GLM for each subject and were then averaged across subjects using a hierarchical random effect model, allowing a generalization of the results to the population level. A second multi-subject GLM analysis was performed to see the direction of connectivity differences between the groups. Map threshold was $p < 0.05$ using Monte Carlo cluster size correction to correct for multiple comparisons ($p < 0.05$).

The first component of the multivariate pattern analysis values in the four significant ROIs were extracted for further between measure analysis.

Correlations Between Measures

As described above, measures were extracted from significant ROIs for further analysis. Spearman correlation tests and multiple linear regression were used to identify the relationship between the different brain measures and between them and MMSE.

Statistical Analysis

SPSS, Excel, Matlab and BrainVoyager statistical tools were used for statistical analysis. Multiple comparisons were corrected using FDR correction or Monte Carlo cluster size correction as detailed above.

Data Availability Statement

The datasets generated for this study are available upon request from the corresponding author.

Results

Structural MRI Data

Bilateral cortical thinning was seen in patients as compared to controls. As expected, the main areas of thinning were bilateral associative visual regions (Broadman 18 and 19), sparing the primary visual area. In these areas cortical thinning was more pronounced on the left hemisphere. However, the right hemisphere exhibited a more diffuse pattern of involvement. This included involvement of additional areas in the visual network: the fusiform gyrus, known to be involved in face recognition; Broadman area 7, known to be involved in spatial localization; and the frontal eye fields (FEF), known to be involved in control of eye movements.

Slight thinning was found in areas outside the visual network, including the primary motor area in both hemispheres, and the primary auditory area and the angular gyrus in the right hemisphere (Table 3 and Fig. 1).

Hippocampus volume comparison between the groups showed a significant reduction in volume in the PCA group on both hemispheres, with the average volume reduction being more pronounced on the left (left: $p = 0.004$; right: $p = 0.009$; Fig. 2).

DTI

The automated method delineated 20 fiber tracks for each subject. In general, almost all fiber bundles were successfully delineated and no difference in the number of delineated fibers was seen between the groups (Supplementary Table 1).

Differences between diffusivity measures in PCA patients and controls, along the tract profiles were assessed.

Analysis of diffusivity measures along the length of each fiber did not detect any affected segments throughout the fibers, excluding three fibers on the left (Supplementary Fig. 1). Significant reduction in FA was found in two visual-related tracts—the left inferior longitudinal fasciculus (points 19–29 cluster size corrected; 36–41

Table 3 Cortical thickness areas in MNI coordinates

Cortical thickness					
Right			Left		
Area	MNI	P (FWE corrected)	Area	MNI	P (FWE corrected)
BA19 V2	47, -81, 4	0.000	Visual association BA 18	44, -83, -1	0.000
Visual Association BA 18	23, -55, -1	0.004	Visual parietal cortex	-39, -45, -36	0.007
Visual association BA 19	7, -78, 29	0.012	BA 39 angular gyurs	-58, -47, -26	0.002
FFG	64, -50, -1	0.005	BA 6 primary motor	-41, -7, 46	0.022
BA 8 FEF	39, 24, 42	0.005			
BA 7 Spatial location	30, -49, 44	0.002			
	14, -75, 45				
BA 6 Primary motor	45, 2, 33	0.004			
BA 21	53, -30, -9	0.003			
Primary auditory	49, -33, 13	0.004			

BA broadman area, MNI montreal neurological institute, FFG fusiform gyrus, FWE family wise estimation

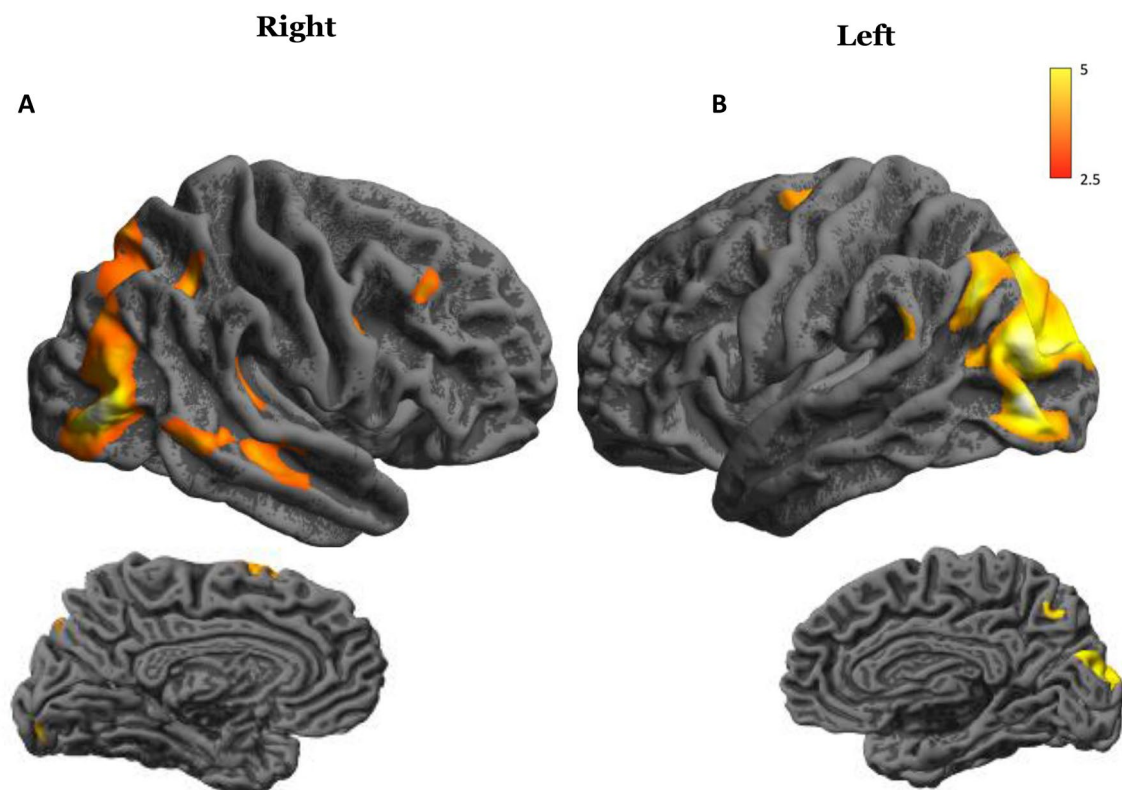
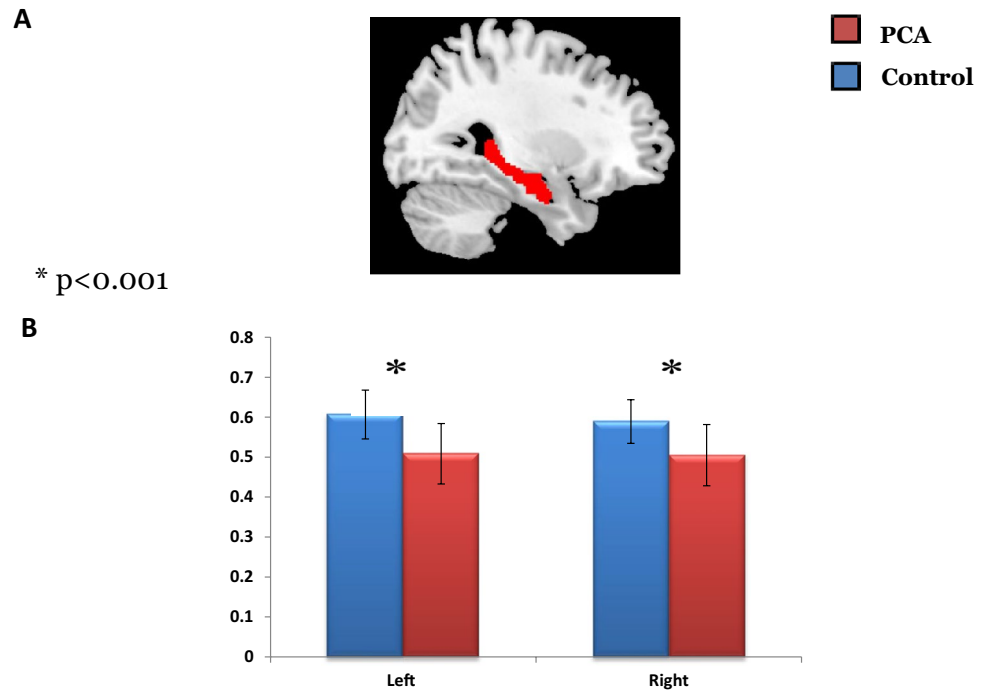


Fig. 1 Cortical thickness. Maps showing reduction in cortical thickness in PCA patients compared to controls. The color bar corresponds to the t values, the lighter the color, the worse the atrophy. Threshold Significance was set at $p < 0.05$ (corrected for FWE)

pointwise FWE p corrected) and the left side of the forceps major (points 3–6 pointwise FWE p corrected; 17–27 cluster size corrected). The average FA along these fibers was correlated in patient group but not in controls (patient group Spearman correlation 0.762, $p < 0.03$; control group Spearman correlation 0.44, $p = 0.13$ n.s.). The other fiber

with an affected segment is related to memory functions—the left cingulate hippocampus fiber (points 17–39, cluster size corrected) (Fig. 3). In these fibers no scanner type effect was found ($p > 0.05$ for all points in all fibers). No significant differences were found in any of the fibers for the other diffusivity measures.

Fig. 2 Hippocampal volume. **a** Hippocampal region, marked in red, used for volume-based morphometry (VBM). **b** Comparison of average volume of the hippocampus (controls in blue and patients in red). Error bar indicates standard deviation. Both hippocampi were significantly different ($p < 0.01$)



Resting State fMRI

The MVPA analysis revealed four significantly different clusters located in the left and right Brodman area (BA) 19, the right BA 37 (fusiform gyrus), and the right BA 39 (Fig. 4). When using these clusters as seeds for connectivity analysis, reduced connectivity was found in the PCA patients for the first three clusters (right and left BA 19 and right BA 37) throughout the brain. On the other hand, right BA 39 showed a mixed pattern—decreased connectivity with the posterior visual regions but increased connectivity with the frontal areas in the PCA patients (Fig. 5).

Correlations Between Measures

The average FA in the left part of the forceps major was correlated with cortical thickness in the left LO region (Spearman 0.495 $p < 0.03$) and rSMG (Spearman 0.483 $p < 0.035$). The FA in the left ILF was correlated with the cortical thickness of the rSMG (Spearman 0.492, $p < 0.017$). Adding both group and FA in the left part of the forceps major and the left ILF to a regression model showed that the effect is influenced by group factor ($t = 3.66$ $p < 0.002$) while FA in either fiber did not contribute significantly to the model (rSMG: $F(16.3) = 5.905$ $p < 0.007$, $t(\text{group}) = 3.66$ $p < 0.002$; left LO: $F(16.3) = 14.450$ $p < 0.001$, $t(\text{group}) = 5.529$ $p < 0.001$).

The connectivity level of the right Brodman area 37 was correlated with the cortical thickness in the left IP region (Spearman 0.539 $p < 0.008$), and right LG (Spearman 0.508 $p < 0.013$). When limiting the analysis to the patient

group only, correlations were significant with left IP region (Spearman 0.733 $p < 0.025$) and rSMG (Spearman 0.767 $p < 0.016$).

The connectivity level of the Right Brodman area 19 was correlated with the cortical thickness in the left IP region (Spearman 0.552 $p < 0.006$), rSMG (Spearman 0.474 $p < 0.022$) and the right LG (Spearman 0.486 $p < 0.019$). When limiting the analysis to the patient group only, correlations were significant with left IP region (Spearman 0.767 $p < 0.016$) and rSMG (Spearman 0.767 $p < 0.016$).

Within patient group, MMSE was slightly correlated with connectivity of right Brodman 19 (Spearman 0.757 $p < 0.05$), cortical thickness of the left IP region (Spearman 0.793 $p < 0.033$) and the Hippocampal volume (right hippocampus: Spearman 0.757 $p < 0.05$; left hippocampus: Spearman 0.739 $p = 0.058$ n.s.).

Discussion

To summarize, multi-modal structural and functional holistic assessment of early-stage PCA patients' brains highlight the local aspects of the disease, with clear selective deficits in the visual and memory-related areas. These results correspond with our previous work (Glick-Shames et al. 2018), in which we scanned the same cohort of patients, honing its conclusions. These findings are specifically intriguing in context of the global analysis conducted in this paper. While in our early work on PCA patients, we concentrated on the vicinity of the visual system, and so it was not surprising

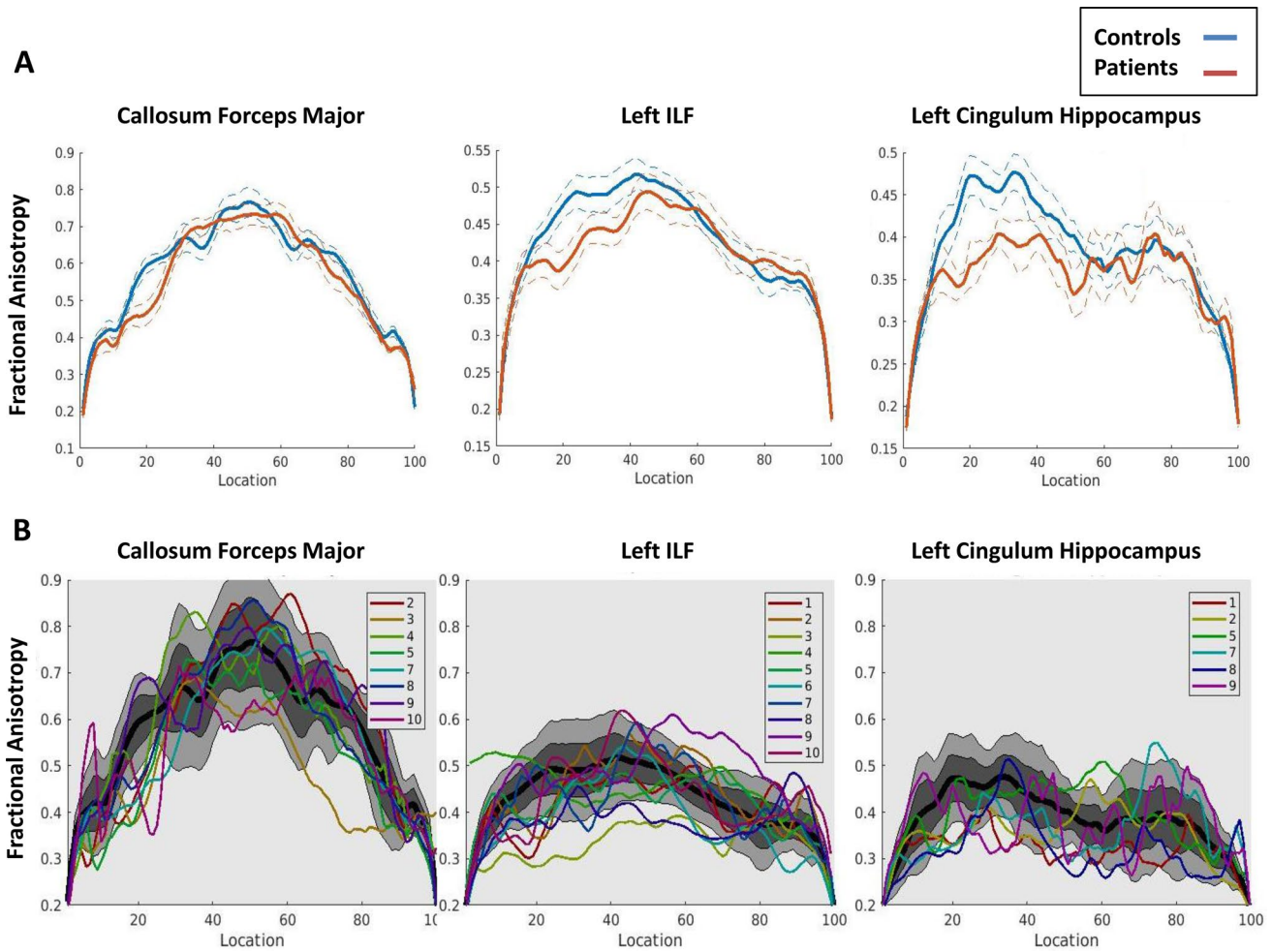
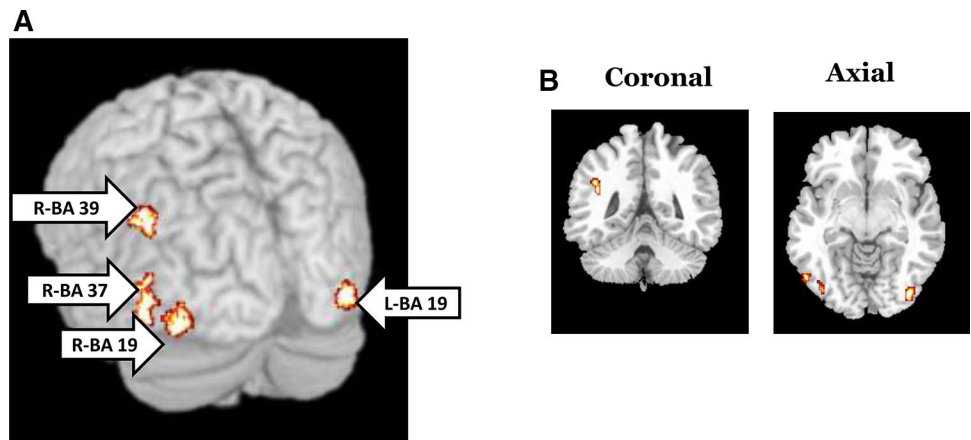


Fig. 3 Fractional anisotropy (FA) along the affected fibers. **a** Average FA along the Forceps Major, Left ILF, and Left Cingulum Hippocampus (controls in blue and patients in red). Standard deviations for each group are marked by dashed lines. The values for Forceps Major are presented from left to right. Values of Left ILF and Left

Cingulum Hippocampus are presented from anterior to posterior. **b** Fibers are presented superimposed on a sagittal T1 image. Statistical differences (p value of t -test) between groups are presented on a representation of the core-fiber to demonstrate the location of between group differences

Fig. 4 Global connectivity clusters. The four clusters of differential connectivity identified using MVPA are superimposed on a whole brain template (**a**) and on axial and coronal slices (**b**)



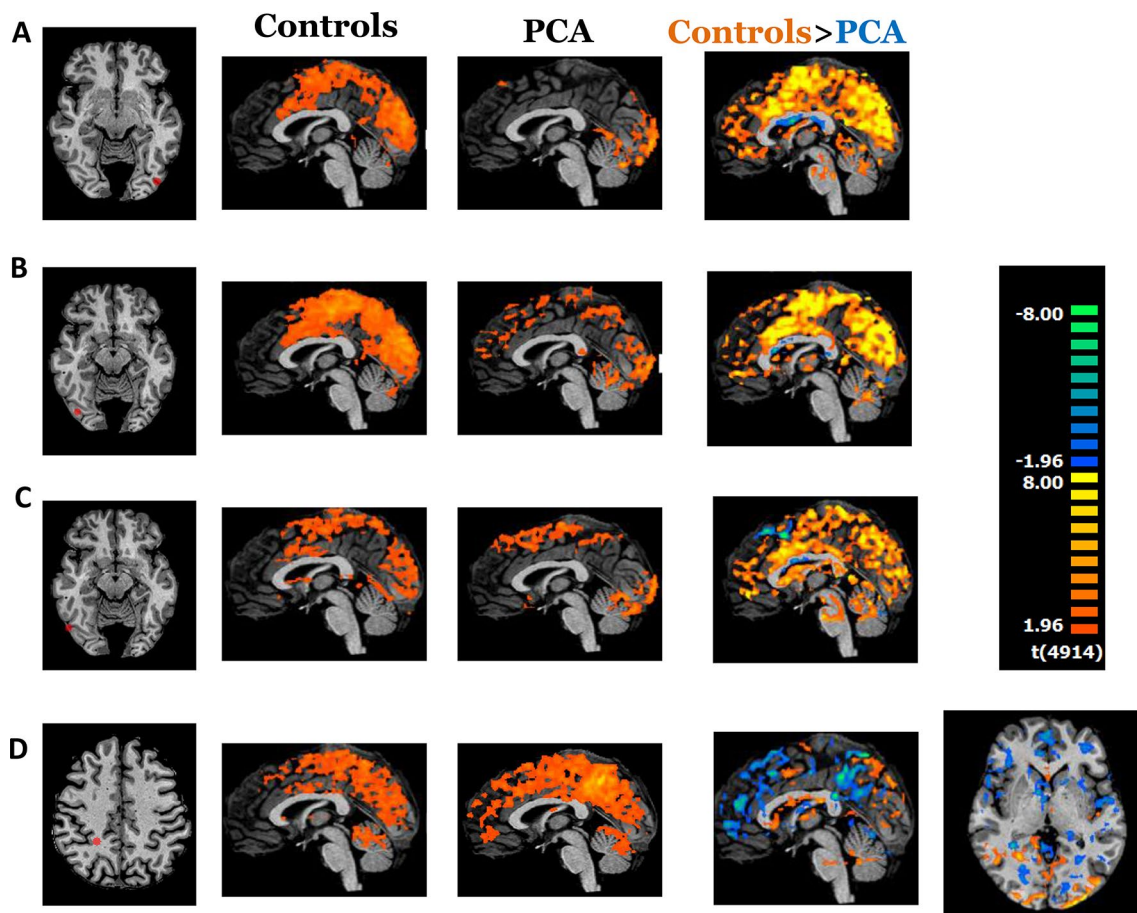


Fig. 5 Seed region connectivity map. Seed regions are presented on T1 images of one individual brain. Connectivity maps for controls and PCA patients, and the subtraction map are all random effect maps

with the threshold set at $p < 0.05$ corrected for multiple comparisons **a** Left BA 19, **b** Right BA 19, **c** Right BA 37, **d** BA 3

that we found specific deficits in these areas, herein we report the damage to be very local even when considered from a whole-brain point-of-view.

Specifically, cortical thinning was evident primarily in the higher visual areas while the primary visual cortex was relatively spared. This goes hand in hand with previous research (Lehmann et al. 2011) and compliments our previous findings showing similar pattern of reduction in brain volume (Glick-Shames et al. 2018). Additionally, although patient insight and memory seemed relatively preserved, hippocampal volume was significantly reduced as compared to age-matched controls. Correspondingly, white matter involvement that was evaluated in all major fiber tracts (within and outside the visual system) was found only in fibers related to associative visual areas and in hippocampal-related fibers. Previous research, limited to the visual system, elicited similar results (Migliaccio et al. 2012; Cerami et al. 2015; Glick-Shames et al. 2018). It is important to note that the forceps major, reported here to be affected in the patients, is the same as the occipital callosal fiber tract which we reported

to be affected in our previous paper. Thus, within the same cohort, although the method differs, the findings coincide and in both studies reduced FA in the central section of the left part of the forceps major was reported. (Glick-Shames et al. 2018). Correlations were found between cortical thickness and fibers integrity, however the presence of disease seems to be the significant factor rather than the specific pattern of grey matter damage. To that end we suggest that independent involvement of white matter in PCA may exist, beyond what is expected from neighboring grey matter atrophied regions.

Finally, global connectivity changes were also relatively local, expressing reduced connectivity in the associative visual areas. As expected, this reduced connectivity was correlated to the atrophy level, matching previous reports. (Adriaanse et al. 2014; Lehmann et al. 2015; Glick-Shames et al. 2018).

Interestingly, a subtle increase in connectivity was detected between BA39 and frontal areas. Moreover, the connectivity in this region showed no correlation with

cortical thinning, suggesting that the alteration does not originate directly from the disease-related damage but rather through an alternative mechanism. This increased connectivity goes along with previous research in AD that found increased connectivity in the anterior DMN (Damoiseaux et al. 2012) and may point to some aspects of plasticity mechanisms outside the affected network or, alternatively, may be an initial sign of network dysfunction (Migliaccio et al. 2016).

Studies have found that AD is the most common underlying cause of disease in PCA (Crutch et al. 2017). The known pathologies of AD, A β senile plaques and tau tangles, as well as elevated tau in the CSF (Montine et al. 2012), have all been reported in PCA (Tang-Wai et al. 2004; Lehmann et al. 2013; Teng et al. 2014). Even so, the clinical picture of the variants is very different. PCA patients are characterized by decline in visual function with relatively preserved memory, language and inter-personal functions (Alves et al. 2015; Crutch et al. 2017). AD patients, on the other hand, are characterized by memory impairment and cognitive decline (Montine et al. 2012). Correspondingly, the anatomical signature (atrophy) in PCA patients highlights parietal and occipital involvement (Benson et al. 1988; Maia da Silva et al. 2017), while AD patients' exhibit atrophy in medial temporal lobe structures (Duara et al. 2008).

This selective involvement of the posterior areas in PCA patients raises a question about the cause of the specific spread of disease. The fact that the same type of pathology causes such different clinical manifestations encouraged extensive research on this topic (Warren et al. 2012) and several different explanations have been proposed. The first suggested culprit was A β accumulation, since studies showed slightly increased occipital A β accumulation in PCA patients compared to other AD patients (Lehmann et al. 2013). However, other autopsy studies failed to replicate this regional pattern and showed that A β accumulation spread does not differ significantly in the different variants of AD and provides surprisingly little information about AD phenotypes (Rosenbloom et al. 2011; Walker and Jucker 2015). Correspondingly, an in vivo research using PET C-PiB (amyloid- β) biomarkers also did not find regional correlation between areas with increased C-PiB and areas with reduced [F]FDG uptake or clinical manifestations (Ossenkuppele et al. 2016).

A more promising pathological option to explain the paradox is the distribution of neurofibrillary tangles. Tau tangles spread seems to be more closely related to distribution of atrophy and clinical symptoms than A β (Mitchell et al. 2002). Tau pathology also seems to precede A β pathology (Jack and Holtzman 2013). Tau tangles were found in occipital and parietal cortices of patients with PCA (Tang-Wai et al. 2004). The development of tau FDG-PET imaging allows this to be tested in living patients as well. A recent study of AD variants found a

regional correlation between [F] AV-1451 (tau biomarker), decreased [F] FDG uptake (Ossenkuppele et al. 2016) and clinical manifestation.

A different approach to explain the involvement of specific areas in AD variants, such as PCA, is the network theory, since the AD variants map very broadly onto well-established known networks (Zhou et al. 2012). Based on this, the neuro-degenerative network theory was suggested to encompass all of the above findings: diffuse spread of A β , specific distribution of tau tangles and specific network involvement. This theory is based on correlation-based connections between preexisting deficits prior to degeneration and the affected network (Miller et al. 2013, 2018). Thus, A β accumulation is driven by total neuronal activity, while tau pathology begins in a prodromal vulnerable area and spreads trans-neuronally to close, or connected networks.

Our current findings, of cortical thinning in the associative visual areas and corresponding selective involvement of higher visual networks, as well as our previous research examining connectivity within the visual network (Glick-Shames et al. 2018), show that reduction in connectivity in PCA patients goes hand in hand with areas of atrophy, thus supporting this notion.

Beyond the suggested role in the spread of disease, functional networking was also described as part of brain mechanism to overcome damage. This was suggested in AD (Damoiseaux et al. 2012; Badhwar et al. 2017) and in PCA (Migliaccio et al. 2016), as well as in other diseases affecting the visual system (Backner et al. 2018)).

Further, it is important to note in this context, that beyond the functional aspect of networking which relates to correlation of activation, networking is also affected by the integrity of the white matter. It was previously suggested that impaired white matter integrity precedes atrophy (Stricker et al. 2013). Our findings specifically highlight the selective involvement of white matter in the disease. Only visual and memory fibers were involved. This corresponded to visual areas of cortical thinning and hippocampal atrophy which were detected in the patients. However, areas that demonstrated cortical thinning were slightly more diffuse than those showing fiber involvement. For example: even though there was some thinning in BA 6, the primary motor area, no specific effects were found in the cortical spinal tract. Thus, pointing to a subordinate role of the white matter rather than it being the primary player. However as cortical thickness did not significantly contribute to the white matter damage beyond existence of disease, it seems that PCA is directly involved in white matter and these effects are not merely a result of damage to grey matter. It should be noted that the lack of observed effects may also stem from the small cohort size and longitudinal studies in a larger cohort are necessary to fully describe the involvement of white matter in the predominantly grey matter disease.

Our findings of selective involvement even within the affected visual network (specifically, the bilateral sparing of the primary visual area), bring forth further thoughts of causes of selective spread in neuro-degenerative disease. It was suggested that specific cell types may be differently vulnerable to damage (Yong et al. 2016). For example, complex cells in V4 are more prone to degeneration than simple cells in V1. Axon length was also suggested to explain selective susceptibility of different neurons to degeneration: cells with long axons (like in Brodmann areas 18 and 19) were reported to be more sensitive than cells with shorter axons (von Gunten et al. 2006).

The low number of patients limits our statistical power and therefore findings may include false negatives. However the low incidence of the disease (affecting only 5% of AD patients) entails conducting such studies in limited cohorts. The cross-sectional design does not allow evaluation of degeneration spread along the course of disease and to that end a follow-up longitudinal study is required. It is also important to note that our patients were diagnosed mainly clinically and that biomarkers to confirm pathology were available only on a subset of patients (Table 1). Another drawback is the fact that the data was collected on two different scanners. To ensure that the scanner did not affect the results, controls were selected to create balanced groups from both scanners. Furthermore, the scanner type was included in analysis and was not a significant confounding factor in any of the results. And finally, the laterality discrepancy between the white matter and connectivity results should be taken into account. All white matter effects were in the left hemisphere, while more loci of functional connectivity changes were found in the right hemisphere. Similarly, while we found greater thinning of the cortex in the left hemisphere, larger areas were affected in the right hemisphere. As no clear laterality was reported in other studies (Millington et al. 2017), and due to the relatively small cohort size, it is impossible to determine whether our results suggest a complex bilateral pattern, or that additional patients would allow the emergence of a clear and consistent lateralization.

Conclusion

Herein we emphasized, using multimodal global imaging methods, the highly localized nature of PCA. Selective involvement was found within the associative visual and memory networks. In these networks the reduction in cortical thickness went hand in hand with the decrease in connectivity. The functional networks seem to play a role in the spread of disease, but may also point to reorganization patterns in spared networks where connectivity is altered with no correlated anatomical damage. The involvement of the

white matter seems to be limited, suggesting a consequential effect, however not directly mediated by grey matter damage. Longitudinal studies are needed to better highlight the interesting interplay between different brain components in this disease.

Compliance with Ethical Standards

Conflict of interest Haya Glick Shames, Tarek Keadan, Yael Backner, Atira Bick, Netta Levin, reports no disclosures or conflicts of interest.

Ethical Approval All procedures performed in studies involving human participants were in accordance with the ethical standards of the institutional and/or national research committee and with the 1964 Helsinki declaration and its later amendments or comparable ethical standards. The Hadassah Hebrew University Medical Center Ethics Committee approved the experimental procedure.

Informed Consent Written informed consent was obtained from all individual participants included in the study.

References

- Adriaanse SM, Sanz-Arigitá EJ, Binnewijzend MA, Ossenkuppele R, Tolboom N, van Assema DM et al (2014) Amyloid and its association with default network integrity in Alzheimer's disease. *Hum Brain Mapp* 35(3):779–791. <https://doi.org/10.1002/hbm.22213>
- Agosta F, Mandic-Stojmenovic G, Canu E, Stojkovic T, Imperiale F, Caso F et al (2018) Functional and structural brain networks in posterior cortical atrophy: a two-centre multiparametric MRI study. *Neuroimage Clin* 19:901–910. <https://doi.org/10.1016/j.nicl.2018.06.013>
- Ahmed S, Baker I, Husain M, Thompson S, Kipps C, Hornberger M et al (2016) Memory impairment at initial clinical presentation in posterior cortical atrophy. *J Alzheimers Dis* 52(4):1245–1250. <https://doi.org/10.3233/jad-160018>
- Ahmed S, Irish M, Loane C, Baker I, Husain M, Thompson S et al (2018) Association between precuneus volume and autobiographical memory impairment in posterior cortical atrophy: beyond the visual syndrome. *Neuroimage Clin* 18:822–834. <https://doi.org/10.1016/j.nicl.2018.03.008>
- Alladi S, Xuereb J, Bak T, Nestor P, Knibb J, Patterson K et al (2007) Focal cortical presentations of Alzheimer's disease. *Brain* 130(Pt 10):2636–2645. <https://doi.org/10.1093/brain/awm213>
- Alves J, Soares JM, Sampaio A, Goncalves OF (2013) Posterior cortical atrophy and Alzheimer's disease: a meta-analytic review of neuropsychological and brain morphometry studies. *Brain Imag Behav* 7(3):353–361. <https://doi.org/10.1007/s11682-013-9236-1>
- Alves J, Magalhães R, Arantes M, Cruz S, Gonçalves ÓF, Sampaio A (2015) Cognitive rehabilitation in a visual variant of Alzheimer's disease. *Appl Neuropsychol: Adult* 22(1):73–78. <https://doi.org/10.1080/23279095.2013.831865>
- Backner Y, Kuchling J, Massarwa S, Oberwahrenbrock T, Finke C, Bellmann-Strobl J et al (2018) Anatomical wiring and functional networking changes in the visual system following optic neuritis. *JAMA Neurol*. <https://doi.org/10.1001/jamaneurol.2017.3880>
- Badhwar A, Tam A, Dansereau C, Orban P, Hoffstaedter F, Bellec P (2017) Resting-state network dysfunction in Alzheimer's disease: a systematic review and meta-analysis. *Alzheimer's Dement*

- Diagn Assess Dis Monit 8(73–85):2017. <https://doi.org/10.1016/j.dadm.2017.03.007.eCollection>
- Beh SC, Muthusamy B, Calabresi P, Hart J, Zee D, Patel V et al (2015) Hiding in plain sight: a closer look at posterior cortical atrophy. *Pract Neurol* 15(1):5–13. <https://doi.org/10.1136/practneuro-1-2014-000883>
- Benson DF, Davis RJ, Snyder BD (1988) Posterior cortical atrophy. *Arch Neurol* 7:193–203. <https://doi.org/10.1684/pnv.2009.0169>
- Bergeron D, Flynn K, Verret L, Poulin S, Bouchard RW, Bocti C et al (2017) Multicenter validation of an MMSE-MoCA conversion table. *J Am Geriatr Soc* 65(5):1067–1072. <https://doi.org/10.1111/jgs.14779>
- Birch EE, Salomão S (1998) Infant random dot stereoacuity cards. *J Pediatr Ophthalmol Strabismus* 35(2):86–90
- Caso F, Agosta F, Mattavelli D, Migliaccio R, Canu E, Magnani G et al (2015) White matter degeneration in atypical Alzheimer disease. *Radiology* 277(1):162–172. <https://doi.org/10.1148/radiol.2015142766>
- Cerami C, Crespi C, Della Rosa PA, Dodich A, Marcone A, Magnani G et al (2015) Brain changes within the visuo-spatial attentional network in posterior cortical atrophy. *J Alzheimers Dis* 43(2):385–395. <https://doi.org/10.3233/JAD-141275>
- Cole BL, Lian KY, Lakkis C (2006) The new Richmond HRR pseudo-isochromatic test for colour vision is better than the Ishihara test. *Clin Exp Optom* 89(2):73–80
- Crutch SJ, Schott JM, Rabinovici GD, Murray M, Snowden JS, van der Flier WM et al (2017) Consensus classification of posterior cortical atrophy. *Alzheimers Dement* 13(8):870–884. <https://doi.org/10.1016/j.jalz.2017.01.014>
- Damoiseaux JS, Prater KE, Miller BL, Greicius MD (2012) Functional connectivity tracks clinical deterioration in Alzheimer's disease. *Neurobiol Aging* 33(4):828.e19–30. <https://doi.org/10.1016/j.neurobiolaging.2011.06.024>
- Duara R, Loewenstein DA, Potter E, Appel J, Greig MT, Urs R et al (2008) Medial temporal lobe atrophy on MRI scans and the diagnosis of Alzheimer disease. *Neurology* 71(24):1986–1992. <https://doi.org/10.1212/01.wnl.0000336925.79704.9f>
- Evans, A. C., Collins, D. L., Mills, S. R., Brown, E. D., Kelly, R. L., Peters, T. M. (1993) '3D statistical neuroanatomical models from 305 MRI volumes' 1993 IEEE Conference Record Nuclear Science Symposium and Medical Imaging Conference. 31 Oct-6 Nov 1993. pp. 1813–1817 vol.3.
- Folstein MF, Folstein SE, McHugh PR (1975) Mini-mental state. A practical method for grading the cognitive state of patients for the clinician. *J Psychiatr Res* 12(3):189–98. [https://doi.org/10.1016/0022-3956\(75\)90026-6](https://doi.org/10.1016/0022-3956(75)90026-6)
- Glick-Shames H, Backner Y, Bick A, Raz N, Levin N (2018) The impact of localized grey matter damage on neighboring connectivity: posterior cortical atrophy and the visual network. *Brain Imaging Behav*. <https://doi.org/10.1007/s11682-018-9952-7>
- Hoffmann M, Keiseb J, Moodley J, Corr P (2002) Appropriate neurological evaluation and multimodality magnetic resonance imaging in eclampsia. *Acta Neurol Scand* 106(3):159–167. <https://doi.org/10.1034/j.1600-0404.2002.01255.x>
- Hua K, Zhang J, Wakana S, Jiang H, Li X, Reich DS et al (2008) Tract probability maps in stereotaxic spaces: analyses of white matter anatomy and tract-specific quantification. *Neuroimage* 39(1):336–347. <https://doi.org/10.1016/j.neuroimage.2007.07.053>
- Jack CR Jr, Holtzman DM (2013) Biomarker modeling of Alzheimer's disease. *Neuron* 80(6):1347–1358. <https://doi.org/10.1016/j.neuron.2013.12.003>
- Kas A, de Souza LC, Samri D, Bartolomeo P, Lacomblez L, Kalafat M et al (2011) Neural correlates of cognitive impairment in posterior cortical atrophy. *Brain* 134(Pt 5):1464–1478. <https://doi.org/10.1093/brain/awr055>
- LaBarge E, Edwards D, Knesevich JW (1986) Performance of normal elderly on the Boston naming test. *Brain Lang* 27(2):380–384. [https://doi.org/10.1016/0093-934x\(86\)90026-x](https://doi.org/10.1016/0093-934x(86)90026-x)
- Lacadie CM, Fulbright RK, Rajeevan N, Constable RT, Papademetris X (2008) More accurate Talairach coordinates for neuroimaging using non-linear registration. *Neuroimage* 42(2):717–725. <https://doi.org/10.1016/j.neuroimage.2008.04.240>
- Lehmann M, Crutch SJ, Ridgway GR, Ridha BH, Barnes J, Warrington EK et al (2011) Cortical thickness and voxel-based morphometry in posterior cortical atrophy and typical Alzheimer's disease. *Neurobiol Aging* 32(8):1466–1476. <https://doi.org/10.1016/j.neurobiolaging.2009.08.017>
- Lehmann M, Ghosh PM, Madison C, Laforce R, Corbetta-Rastelli C, Weiner MW et al (2013) Diverging patterns of amyloid deposition and hypometabolism in clinical variants of probable Alzheimer's disease. *Brain* 136(Pt 3):844–858. <https://doi.org/10.1093/brain/awt327>
- Lehmann M, Madison C, Ghosh PM, Miller ZA, Greicius MD, Kramer JH et al (2015) Loss of functional connectivity is greater outside the default mode network in nonfamilial early-onset Alzheimer's disease variants. *Neurobiol Ag* 36(10):2678–2686. <https://doi.org/10.1016/j.neurobiolaging.2015.06.029>
- Madhavan A, Schwarz CG, Duffy JR, Strand EA, Machulda MM, Drubach DA et al (2016) Characterizing white matter tract degeneration in syndromic variants of Alzheimer's disease: a diffusion tensor imaging study. *J Alzheimers Dis* 49(3):633–643
- Maia da Silva MN, Millington RS, Bridge H, James-Galton M, Plant GT (2017) Visual dysfunction in posterior cortical atrophy. *Front Neurol* 8:389. <https://doi.org/10.3389/fneur.2017.00389>
- Manning EN, Macdonald KE, Leung KK, Young J, Pepple T, Lehmann M et al (2015) Differential hippocampal shapes in posterior cortical atrophy patients: a comparison with control and typical AD subjects. *Hum Brain Mapp* 36(12):5123–5136. <https://doi.org/10.1002/hbm.22999>
- Migliaccio R, Agosta F, Scola E, Magnani G, Cappa SF, Pagani E et al (2012) Ventral and dorsal visual streams in posterior cortical atrophy: a DT MRI study. *NBA* 33(11):2572–2584. <https://doi.org/10.1016/j.neurobiolaging.2011.12.025>
- Migliaccio R, Gallea C, Kas A, Perlberg V, Samri D, Trotta L et al (2016) Functional connectivity of ventral and dorsal visual streams in posterior cortical atrophy. *J Alzheimers Dis* 51(4):1119–1130. <https://doi.org/10.3233/jad-150934>
- Migliaccio R, Agosta F, Basaia S, Cividini C, Habert MO, Kas A et al (2020) Functional brain connectome in posterior cortical atrophy. *Neuroimage Clin* 25:102100. <https://doi.org/10.1016/j.nicl.2019.102100>
- Millington RS, James-Galton M, Maia Da Silva MN, Plant GT, Bridge H (2017) Lateralized occipital degeneration in posterior cortical atrophy predicts visual field deficits. *Neuroimage Clin* 14:242–249. <https://doi.org/10.1016/j.nicl.2017.01.012>
- Miller ZA, Mandelli ML, Rankin KP, Henry ML, Babiak MC, Frazier DT et al (2013) Handedness and language learning disability differentially distribute in progressive aphasia variants. *Brain* 136(Pt 11):3461–3473. <https://doi.org/10.1093/brain/awt242>
- Miller ZA, Rosenberg L, Santos-Santos MA, Stephens M, Allen IE, Hubbard HI et al (2018) Prevalence of mathematical and visuospatial learning disabilities in patients with posterior cortical atrophy. *JAMA Neurol*. <https://doi.org/10.1001/jamaneurol.2018.0395>
- Mitchell TW, Mufson EJ, Schneider JA, Cochran EJ, Nissannov J, Han LY et al (2002) Parahippocampal tau pathology in healthy aging, mild cognitive impairment, and early Alzheimer's disease. *Ann Neurol* 51(2):182–189. <https://doi.org/10.1002/ana.10086>
- Montembeault M, Brambati SM, Lamari F, Michon A, Samri D, Epelbaum S et al (2018) Atrophy, metabolism and cognition in the posterior cortical atrophy spectrum based on Alzheimer's disease

- cerebrospinal fluid biomarkers. *Neuroimage Clin* 20:1018–1025. <https://doi.org/10.1016/j.nicl.2018.10.010>
- Montine TJ, Phelps CH, Beach TG, Bigio EH, Cairns NJ, Dickson DW et al (2012) National institute on aging–Alzheimer’s association guidelines for the neuropathologic assessment of Alzheimer’s disease: a practical approach. *Acta Neuropathol* 123(1):1–11
- Nichols TE, Holmes AP (2002) Nonparametric permutation tests for functional neuroimaging: a primer with examples. *Hum Brain Mapp* 15(1):1–25. <https://doi.org/10.1002/hbm.1058>
- Ossenkuppe R, Schonhaut DR, Scholl M, Lockhart SN, Ayakta N, Baker SL et al (2016) Tau PET patterns mirror clinical and neuroanatomical variability in Alzheimer’s disease. *Brain* 139(Pt 5):1551–1567. <https://doi.org/10.1093/brain/aww027>
- Peng G, Wang J, Feng Z, Liu P, Zhang Y, He F et al (2016) Clinical and neuroimaging differences between posterior cortical atrophy and typical amnesic Alzheimer’s disease patients at an early disease stage. *Sci Rep* 6:29372. <https://doi.org/10.1038/srep29372>
- Rosenbloom M, Alkalay A, Agarwal N, Baker S, O’neil J, Janabi M et al (2011) Distinct clinical and metabolic deficits in PCA and AD are not related to amyloid distribution. *Neurology* 76(21):1789–1796. <https://doi.org/10.1212/WNL.0b013e31821cccad>
- Shames H, Raz N, Levin N (2015) Functional neural substrates of posterior cortical atrophy patients. *J Neurol* 262(7):1751–1761. <https://doi.org/10.1007/s00415-015-7774-8>
- Son SJ, Kim J, Park H (2017) Structural and functional connectional fingerprints in mild cognitive impairment and Alzheimer’s disease patients. *PLoS ONE* 12(3):e0173426. <https://doi.org/10.1371/journal.pone.0173426>
- Stricker NH, Salat DH, Foley JM, Zink TA, Kellison IL, McFarland CP et al (2013) Decreased white matter integrity in neuropsychologically-defined mild cognitive impairment is independent of cortical thinning. *J Int Neuropsychol Soc* 19(8):925–937. <https://doi.org/10.1017/s1355617713000660>
- Tang-Wai DF, Graff-Radford NR, Boeve BF, Dickson DW, Parisi JE, Crook R et al (2004) Clinical, genetic, and neuropathologic. *Neurology* 63:1168–1174. <https://doi.org/10.1212/01.WNL.0000140289.18472.15>
- Teng E, Yamasaki TR, Tran M, Hsiao JJ, Sultzer DL, Mendez MF (2014) Cerebrospinal fluid biomarkers in clinical subtypes of early-onset Alzheimer’s disease. *Dement Geriatr Cogn Disord* 37:307–314. <https://doi.org/10.1159/000355555>
- von Gunten A, Bouras C, Kövari E, Giannakopoulos P, Hof PR (2006) Neural substrates of cognitive and behavioral deficits in atypical Alzheimer’s disease. *Brain Res Rev* 51(2):176–211. <https://doi.org/10.1016/j.brainresrev.2005.11.003>
- Wakana S, Caprihan A, Panzenboeck MM, Fallon JH, Perry M, Gollub RL et al (2007) Reproducibility of quantitative tractography methods applied to cerebral white matter. *Neuroimage* 36(3):630–644
- Walker LC, Jucker M (2015) Neurodegenerative diseases: expanding the prion concept. *Annu Rev Neurosci* 38:87–103
- Warren JD, Fletcher PD, Golden HL (2012) The paradox of syndromic diversity in Alzheimer disease. *Nat Rev Neurol* 8(8):451–464. <https://doi.org/10.1038/nrneuro.2012.135>
- Whitfield-Gabrieli S, Nieto-Castanon A (2012) Conn: a functional connectivity toolbox for correlated and anticorrelated brain networks. *Brain Connect* 2(3):125–141. <https://doi.org/10.1089/brain.2012.0073>
- Yeatman JD, Dougherty RF, Myall NJ, Wandell BA, Feldman HM (2012) Tract profiles of white matter properties: automating fiber-tract quantification. *PLoS ONE* 7(11):e49790. <https://doi.org/10.1371/journal.pone.0049790>
- Yong K, Rajdev K, Warrington E, Nicholas J, Warren J, Crutch S (2016) A longitudinal investigation of the relationship between crowding and reading: a neurodegenerative approach. *Neuropsychologia* 85:127–136. <https://doi.org/10.1016/j.neuropsychologia.2016.02.022>
- Zhou J, Gennatas ED, Kramer JH, Miller BL, Seeley WW (2012) Predicting regional neurodegeneration from the healthy brain functional connectome. *Neuron* 73(6):1216–1227. <https://doi.org/10.1016/j.neuron.2012.03.004>

Publisher’s Note Springer Nature remains neutral with regard to jurisdictional claims in published maps and institutional affiliations.